J. Fluid Mech. (1979), *vol.* 95, *part* 3, *pp.* 515–537
Printed in Great Britain

Flow patterns of large eddies in a wake and in a boundary layer

By A. A. TOWNSEND
Emmanuel College, Cambridge

(Received 15 August 1978)

The turbulent velocity fluctuations at eight positions on sections of a plane wake and a boundary layer have been sampled simultaneously and recorded in digital form on magnetic tape for subsequent numerical analysis. Two configurations have been used (lines of equally-spaced sensors in planes normal to the flow, and arrays with three rows) with sensors responsive both to streamwise and cross-stream components of the fluctuations. To the extent that the Taylor approximation of 'frozen' flow is valid, the recorded fluctuations may be interpreted as instantaneous values at grid points in the volume swept out by the array.

The records have been examined, (*a*) to find evidence for flow patterns with marked periodicity in one direction, and (*b*) to select dimensions and orientations for simple eddy flow patterns whose random superposition would lead to correlation functions with a close resemblance to those calculated from the recorded data. In the wake, clear evidence was found for periodic flow patterns that resemble the eddies of a von Kármán street, but, although the spacing of eddy centres in each group was uniform, it varied considerably from one group to another, suggesting that groups are being observed in different stages of development.

Two kinds of correlation were calculated from the records, (i) simple mean values of velocity products, and (ii) mean values of the products weighted by the total intensity or Reynolds stress in the effective volume swept by the array of sensors. For both kinds, the correlations are well described by simple inclined roller-type eddies, but the correspondence is greatly improved by weighting in favour of intensity or Reynolds stress. It appears that the eddies contributing most to intensity or Reynolds stress are less variable in form than all the eddies together, and that those contributing most to Reynolds stress are significantly different in shape and in orientation from those contributing most to turbulent energy.

1. Introduction

Comparison of correlation functions measured in a wide variety of nearly unidirectional, turbulent shear flows shows that the larger-scale motions that contribute most to turbulent kinetic energy and Reynolds stress have much the same forms in all flows, the principal differences being attributable to 'special' eddies peculiar to individual flows (Townsend 1970). Examples of special eddies are the entrainment eddies in wakes (Grant 1958; Keffer 1965), the transverse or ring vortices in mixing-layers (Bradshaw, Ferriss & Johnson 1964; Brown & Roshko 1974; Davies & Yule 1975; among others), arrays of longitudinal vortices in wall flow (Gupta, Laufer &

0022–1120/79/4337–7820 $02.00

Kaplan 1971), and, in a sense, the overlapping velocity fields of the attached eddies in equilibrium wall layers. Nevertheless, the general similarity is such that the principal differences in mean flow behaviour of the various free turbulent flows, for example, the variation of entrainment constant, can be explained by supposing a basic structural similarity of the turbulent motion.

Most successful schemes for prediction of the development and properties of nearly unidirectional flows are designed to provide an adequate description of the turbulent intensities, stresses and scales as well as the mean flow properties, but they leave open the actual form of the velocity patterns ('eddies') that are responsible for these quantities. The approach is acceptable if the patterns are broadly similar in all flows, but once the velocity gradients of the mean flow depart appreciably from simple shearing the similarity is lost and the ratios of the stresses to turbulent intensity are changed. In effect, an eddy shape parameter, nearly invariant in unidirectional flows, becomes a variable in complex flows and a prediction scheme for these flows should be able to describe in outline the changes of the shape parameter.

The experimental work to be described develops methods for the identification of eddy structures in two unidirectional flows, particularly the structures contributing most to turbulent stresses, turbulent energy and entrainment, using arrays of hot-wire anemometers. Similar measurements in curved and divergent flows would provide a testing-ground for schemes that set out to predict changes of eddy structure as well as the stress ratios.

2. Experimental arrangements

The plane turbulent wakes were produced behind circular cylinders of diameter 9·53 mm in air-streams of velocity around 12 m s^{-1}, giving cylinder Reynolds numbers in the region of 8000, and all the measurements were made at 170 diameters from the cylinder where the distributions of turbulent intensities have become nearly self-preserving in form.

The boundary layer was formed on the floor of a wind-tunnel of square section with sides of 0·45 m. Transition was encouraged by a trip-rod of square section with side 3 mm, placed across the floor at the entrance to the working section. The Reynolds number based on distance from the trip-rod was nearly $1{\cdot}3 \times 10^6$, and the total layer thickness was about 40 mm. Background 'turbulence' was about 0·2 %, mostly in the form of slight surging with mean frequency about 8 Hz.

Turbulent velocity fluctuations were detected by constant-temperature hot-wire anemometers whose outputs were amplified, sampled simultaneously at intervals of 1·024 ms, and recorded on magnetic tape in digital form for subsequent numerical analysis by the Cambridge University IBM 370 computer. The anemometer amplifiers are direct-coupled and their frequency responses are effectively flat from zero frequency to well beyond the maximum significant for the sampling interval used. Most of the records were over a period of 16·4 s (i.e. 16 K readings for each channel), but some longer records were taken to test the internal consistency of the mean values. The data was recorded in the form of eight-bit binary numbers, and the finite discrimination of the conversion would cause over-estimation of variances by $\frac{1}{6}$ bit^2. Typical variances were in excess of 500 and statistical uncertainties are far greater than the systematic error.

The hot-wire sensors were of Wollaston wire, 2·5 μm in diameter and approximately 1 mm long over the etched section, and they were used with two orientations to the flow, normal to the mean flow direction and at 45° to it. The eight sensors were arranged either in a single line or in three parallel lines with two sensors in each outer row and four in the central row. Assuming the validity of the Taylor approximation of 'frozen' flow patterns, the time intervals between successive sample groups correspond with spatial intervals of about 11 mm, and a block of N consecutive groups provides in effect simultaneous values of the velocity fluctuation at $8N$ separate positions within a volume of length $(N-1)\times 11$ mm and cross-section equal to the profile area of the sensor array.

3. Periodic eddy patterns in a cylinder wake

Although photographs of wakes with flow boundaries made visible by injection of dye or smoke show that groups of transverse eddies with axes parallel to the generating cylinder are prominent in the entrainment of ambient fluid (Grant 1958; Keffer 1965), the power spectra show no sign of a peak at the characteristic frequency of eddy passage. A possible reason, suggested by the observations of Gupta *et al.* (1971) in a boundary layer, is that the 'characteristic frequency' is variable, and, although eddies in individual groups may be almost regularly spaced, the spacing varies considerably from one group to the next.

If regularly spaced groups of eddies are present in the flow, it should be possible to obtain significantly good fits of the observed velocity patterns with a model velocity distribution of the expected characteristics. The visualization studies seem to show that the motion in the groups is nearly confined to the $x0z$ plane ($0x$ is in the direction of mean flow and $0z$ in the direction of shear), and is generally similar to an array of spanwise vortices with velocity distribution given by

$$\left.\begin{aligned} u_0(x,z) &= f'(z)\sin kx, \\ w_0(x,z) &= -kf(z)\cos kx, \end{aligned}\right\} \tag{3.1}$$

where k is the wavenumber of variation in the flow direction. The best fit of such a velocity pattern to a recorded block of velocity fluctuations, $u(x,z)$, is $Au_0(x,z)$ where

$$A = \Sigma\, u(x,z)\, u_0(x,z)/\Sigma\, u_0^2 \tag{3.2}$$

and the sum is taken over all the virtual positions of the sensors in the block. From examination of the photographs, it appeared that identifiable groups contained between three and five eddies and so a search was made for patterns that are finite groups covering four complete periods in the $0x$ direction. No reason to change the number developed during the analysis of the records.

Physically, each pattern corresponds to the passage of an organized group of eddies actively engaged in the process of entrainment, and each group must occupy its own region of the flow. If the selectivity of the fitting process is sufficient to discriminate between patterns of different periods, they will cause significantly large values of A at widely separated intervals as patterns of the selected period happen to go by. The main turbulent motion will also contribute to A but that contribution is likely to be normally distributed. Consequently, the probability distribution function for A will be non-Gaussian with values of the kurtosis significantly greater than the normal value of

three, the excess reflecting the intensity of organized eddy groups of the selected period.

To represent a single row of simple eddies, I have used

$$f(z) = \operatorname{sech}[k(z-z_0)], \tag{3.3}$$

where z_0 is the distance of the eddy centres from the central plane of the wake. For a double row that resembles a Kármán eddy street, I use

$$f(z) = \operatorname{sech}[k(z-z_0)] + \operatorname{sech}[k(z+z_0)]. \tag{3.4}$$

These forms are chosen to give zero vorticity, i.e. potential flow, far from the eddy centres.

The convariances, $R_{11}(0,0,r) = \overline{u(x,y,z)\,u(x,y,z+r)}$, shown in figure 1 have been calculated from one set of recorded fluctuations and they are seen to be everywhere positive, unlike the covariances that would arise from an assembly of eddy groups with either of the distribution functions (3.3) or (3.4). The lateral distribution of the longitudinal intensity, $\overline{u^2}$, is consistent in shape and magnitude with results obtained using single sensors (Townsend 1949), indicating that the presence of the array causes little interference with the flow.

For convenience of calculation, the records were analysed by selecting a value for the wavenumber k and then calculating the variance and kurtosis of the coefficient A for various values of the centre displacement z_0. Typical variations of the variance, $\overline{A^2}$, and the kurtosis, $\overline{A^4}/(\overline{A^2})^2$, are shown in figure 2, and it will be seen that the kurtosis has a well-defined maximum for kz_0 in the range 1·2–1·6 while the variance takes a minimum value for a slightly larger value of kz_0. The reason for the minimum of the variance is that the main turbulent motion seems to be composed of simple eddies with instantaneous distributions of velocity of the same sign at all the sensors (figure 1). Since the velocity patterns are of the form, $u_0 = f'(z)\sin kx$, they weight the sum of equation (3.2) both positively and negatively for sensor positions in the region of large intensity and can discriminate against fluctuation patterns that give velocity fluctuations of the same sign at all the sensors. To a considerable extent, the minimum variance depends on rejection of the contribution to A from the main turbulent motion when the sum of the values of $f'(z)$ at the sensor positions is zero.

That a significant component of the velocity field is composed of non-overlapping groups of eddies is shown by records of the sum,

$$S = \sum_{z} \sum_{\substack{x \text{ for} \\ \text{one period}}} u(x,z)\,u_0(x,z), \tag{3.5}$$

in effect the coefficient A for an eddy pattern with a single member (figure 3). By using only one period rather than four, the selectivity of the numerical filter is so low that aperiodic components, e.g. from the main motion, cannot generate periodic transients in the record. Almost the whole of the record consists of regular groups of three to five oscillations, confirming the initial choice of four, and each group is fairly uniform in period although that period varies considerably from one group to the next. Notice that only a small fraction of the record consists of irregular oscillations of the kind that would be produced by overlap or superposition of groups of different periods or by the comparatively simple eddy structures of the main motion. Such records offer clear evidence that non-overlapping eddy groups exist in the flow with a range of

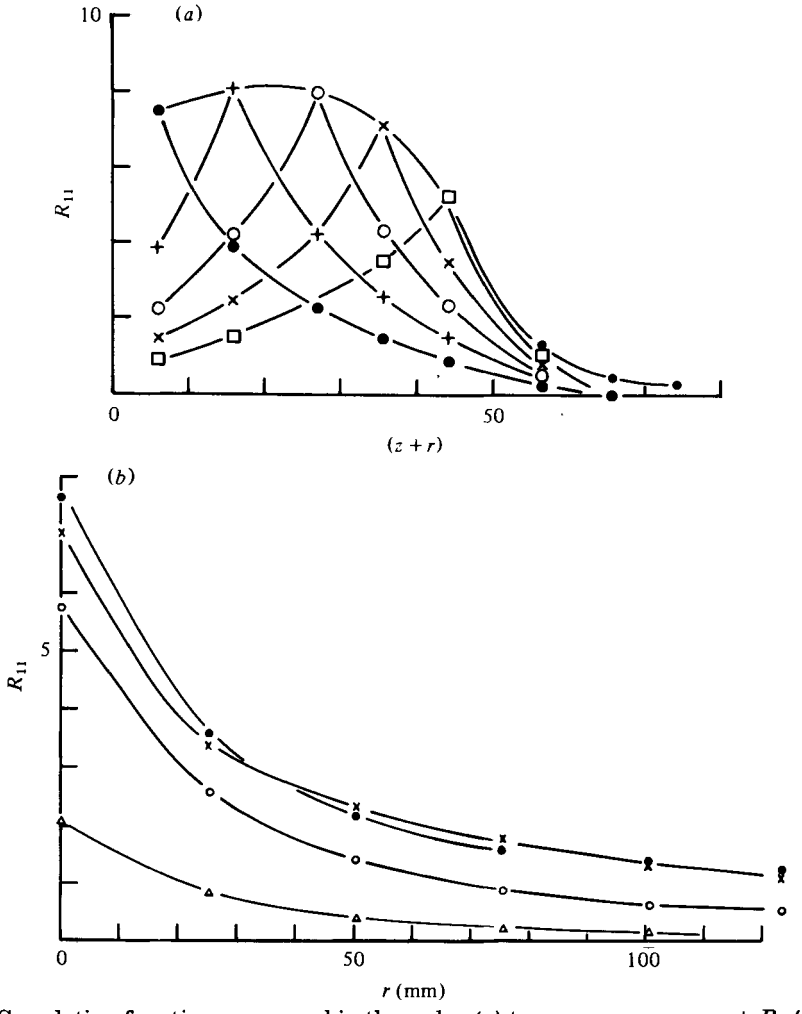

FIGURE 1. Correlation functions measured in the wake, (*a*) transverse component $R_{11}(0, 0, r; z)$; (*b*) longitudinal component $R_{11}(r, 0, 0; z)$. (Units of R_{11} are $10^{-4}U_1^2$.) ×, $z = -1{\cdot}7$; ●, $z = 21{\cdot}3$; ○, $z = 41{\cdot}0$; △, $z = 60{\cdot}3$.

periods and with lateral distributions of velocity similar to those leading to maximum kurtosis of A.

Simple eddy groups with velocity distributions of the form (3.1) do not contribute to the Reynolds stress and cannot exchange energy with the mean flow. A distribution that can exchange energy is defined by

$$\left.\begin{aligned} u_0(x,z) &= f'(z)\sin kx + g'(z)\cos kx, \\ w_0(x,z) &= -kf(z)\cos kx + kg(z)\sin kx, \end{aligned}\right\} \tag{3.6}$$

for which the mean value of the product $u_0 w_0$ over a period is

$$\overline{u_0 w_0} = \tfrac{1}{2}k(f'g - fg'). \tag{3.7}$$

Velocity distributions consistent with the basic concept of simple groups of eddies are provided by

$$\left.\begin{aligned} f(z) &= \operatorname{sech} k(z-z_0) + \operatorname{sech} k(z+z_0), \\ g(z) &= \alpha[\sinh k(z-z_0)\operatorname{sech}^2 k(z-z_0) - \sinh k(z+z_0)\operatorname{sech}^2 k(z+z_0)], \end{aligned}\right\} \tag{3.8}$$

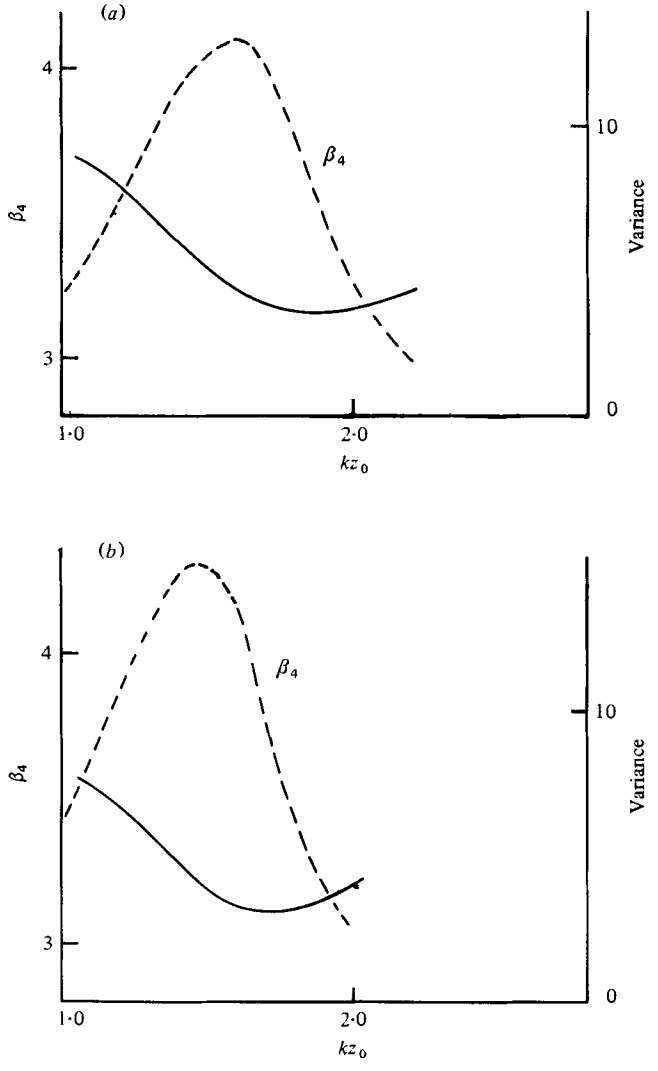

FIGURE 2. Kurtosis β_4 and variance of the pattern coefficient A as functions of eddy centre displacement at constant wave-number. (*a*) Period 10 ms, $k = 0{\cdot}174\ \text{mm}^{-1}$; (*b*) period 12 ms, $k = 0{\cdot}145\ \text{mm}^{-1}$.

and then

$$\overline{u_0 w_0} = -\tfrac{1}{2}\alpha k[\operatorname{sech}^4 k(z-z_0) - \operatorname{sech}^4 k(z+z_0) + 2\operatorname{sech} k(z-z_0)\operatorname{sech}^3 k(z+z_0) - 2\operatorname{sech}^3 k(z-z_0)\operatorname{sech} k(z+z_0)]$$

giving maximum stress near the line of eddy centres.

Using these distribution functions for the calculation of A, the criterion of maximum kurtosis can be used to find optimum values of the displacement z_0 and the stress coefficient α for a particular value of the wavenumber. Figure 4 shows the dependence upon wavenumber of (*a*) the stress coefficient, (*b*) the variance of the convolution quantity A, the maximum value of the kurtosis of A, and (*d*) kz_0, defining the average distance of the eddy centres from the central plane of the wake. Since eddy groups of

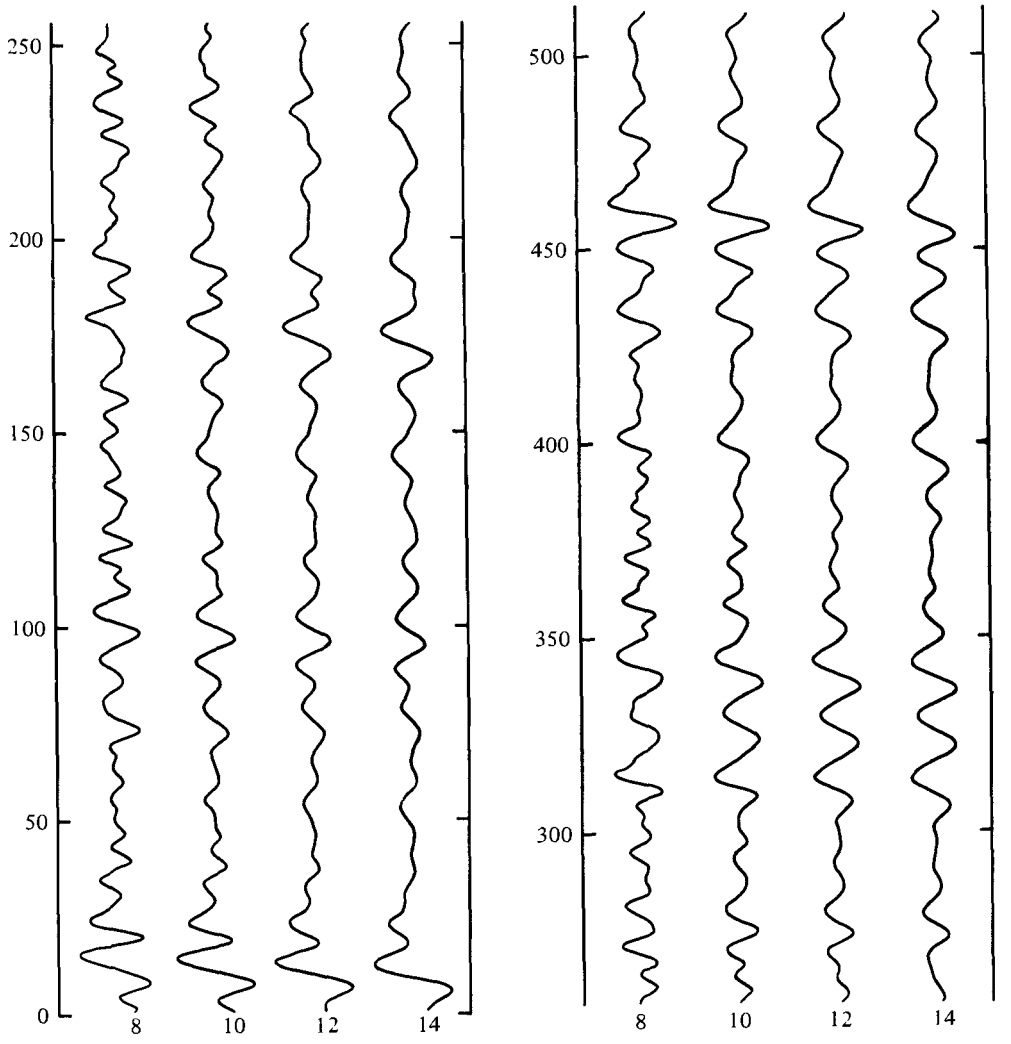

FIGURE 3. Time records of the fluctuation sum S, defined by equation (3.5), for a range of central wavenumber. The numbers below each record specify the period in milliseconds used to form the sum S of equation (3.5).

a particular wavenumber are moderately rare events, the scatter in the values of α for maximum kurtosis is considerable, but there is a discernible trend for values to become more negative for larger values of kz_0. It appears that the sign of the energy transfer from the mean flow to the periodic eddies may reverse at a wavenumber near $130\,\mathrm{m}^{-1}$.

If contributions from the main motion are small, the variance $\overline{A^2}$ is a measure of the contribution to $\overline{u^2}$ by eddy groups whose wavenumbers lie within a range of about 25 % around the selected wavenumber, and figure 4(*b*) shows that smaller eddies of larger wavenumber have more energy than larger ones. The results are in agreement with the view that eddies of wavenumber greater than $130\,\mathrm{m}^{-1}$ belong to 'old' groups generated far upstream and are being observed near the end of their growth cycle with zero or negative growth rate. Eddy groups of smaller wavenumber are in the early

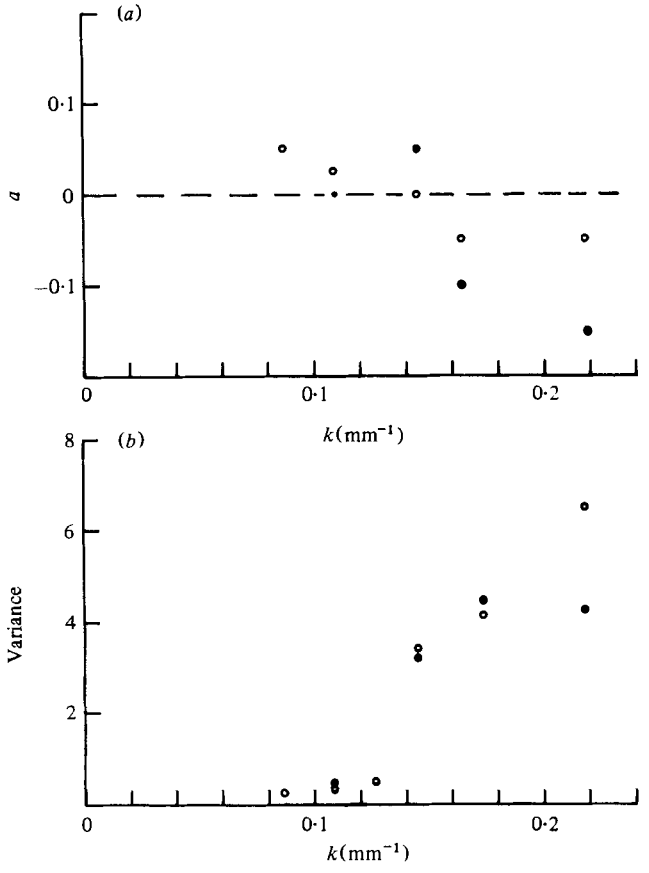

FIGURE 4. For legend see facing page.

stages of growth and have less energy. They are receiving energy from the mean flow and, since they began to develop when the wake width was almost the current size, their centres are further from the central plane.

It is not easy to say how much energy resides in the motion of the eddy groups, but, on the basis that the maximum local contribution to $\overline{u^2}$ from an eddy group with coefficient A is $A^2/8$, the fraction of the total turbulent energy is estimated as between 15 and 20%.

Streamlines of a single eddy of a group are shown in figure 5 for a stress coefficient of 0·1.

4. Long eddies in a boundary layer

The persistent lateral variations of surface stress and mean velocity that have been found in boundary layers (for example, Bradshaw 1965; Fernholtz 1964) probably arise from long roller eddies with axes aligned with the mean flow. The location of the long eddies depends on details of the upstream flow, but it is so difficult to remove the variations that it appears likely that a large-scale flow instability is present, the upstream disturbance acting as the trigger for growth. A possible mechanism of the instability (Townsend 1976) involves the changes in the normal Reynolds stresses

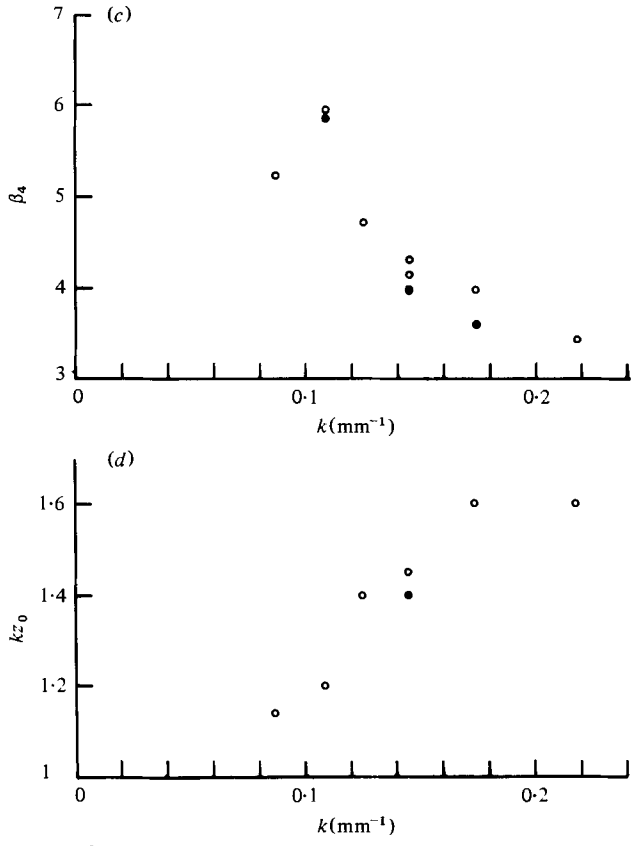

FIGURE 4. Parameters of the periodic eddies of the wake for various wavenumbers: (*a*) Stress coefficient a; (*b*) variance $\overline{A^2}$; (*c*) kurtosis β_4; (*d*) centre displacement kz_0.

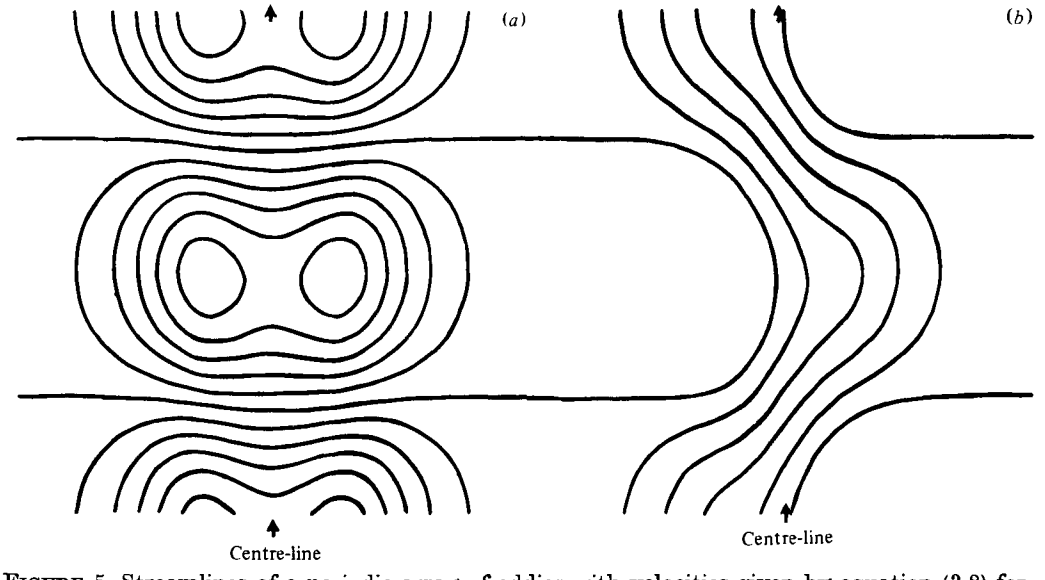

FIGURE 5. Streamlines of a periodic array of eddies with velocities given by equation (3.8) for $kz_0 = 1{\cdot}4$ and $a = 0{\cdot}1$, (*a*) for the eddy motion alone, and (*b*) combined with an error-law distribution of mean velocity and moving with the free stream.

caused by the motion, and it indicates that the flow is unstable to the development of arrays of roller eddies with wavenumbers of lateral periodicity covering a moderate range. If the instability exists, it is likely that periodic groups of roller eddies occur transiently with similar centre spacings. Since each group depends for its energy supply on its organized structure, only one can be present in any particular place and their presence may be detected by techniques analogous to those used for the periodic eddies of the wake.

An attempt has been made to find evidence of groups of longitudinal roller eddies, using records from linear arrays of eight sensors in a line parallel to the surface and at right-angles to the mean flow. Numerical results have been obtained by calculating the Fourier coefficients,

$$C(k_2, t_s) = \sum_{n=1}^{8} \sum_{r=0}^{N-1} u_n(t) \exp(ik_2 y_n), \tag{4.1}$$

where $u_n(t)$ is the fluctuation recorded by the nth sensor at sample time $t_s + r\tau_s$ (τ_s is the interval between samples). The procedure is equivalent to obtaining the best fit to a velocity pattern, $u_0(x, y) = \exp(ik_2 y)$, limited to a range in x of $NU\tau_s$. Calculations of the variance of C, CC^*, and of its kurtosis, $\beta_4 = \overline{(CC^*)^2}/(\overline{CC^*})^2$, are displayed in figure 6.

If non-overlapping, laterally periodic groups of long eddies are present, large values of CC^* will occur when a group with the selected wavenumber and with length comparable with $NU\tau_s$ is within the sampled volume. If the length of the eddies is large compared with the sample length, their contributions to C will be proportional to the sample length and the contributions to its variance proportional to its square. If their length is much smaller than the sample length, each eddy group contributes a constant amount and the variance is proportional to the sample length.

The definition of kurtosis of C is that appropriate to a complex random variable, and the normal value for a Gaussian distribution is two not three. Writing

$$C(t) = a(t) + ib(t)$$

where a and b are real, we have

$$CC^* = a^2 + b^2, \quad (CC^*)^2 = a^4 + b^4 + 2a^2b^2.$$

If a and b are statistically independent and normally distributed,

$$\langle a^2 \rangle = \langle b^2 \rangle, \quad \langle a^2 b^2 \rangle = \langle a^2 \rangle \langle b^2 \rangle, \quad \langle a^4 \rangle = 3\langle a^2 \rangle^2,$$

and so

$$\beta_4 = \langle (CC^*)^2 \rangle / (\langle CC^* \rangle)^2 = 2. \tag{4.2}$$

Since the Fourier transform of equation (4.1) is based on just eight data values, the spectral resolution is far from good, but two ranges of wavenumber can be distinguished:

(*a*) For wavenumbers near $0{\cdot}24\,\mathrm{mm}^{-1}$, the kurtosis is above the normal value of two, and the variance is roughly proportional to N, the number of samples, for N greater than eight. The behaviour of the variance indicates that eddies with these values of the transverse wavenumber have effective lengths in the flow direction of roughly 80 mm.

(*b*) Both the variance and the kurtosis take maximum values for wavenumbers in the range $0{\cdot}10$–$0{\cdot}14\,\mathrm{mm}^{-1}$ (dependent to some extent on the sample number), and the

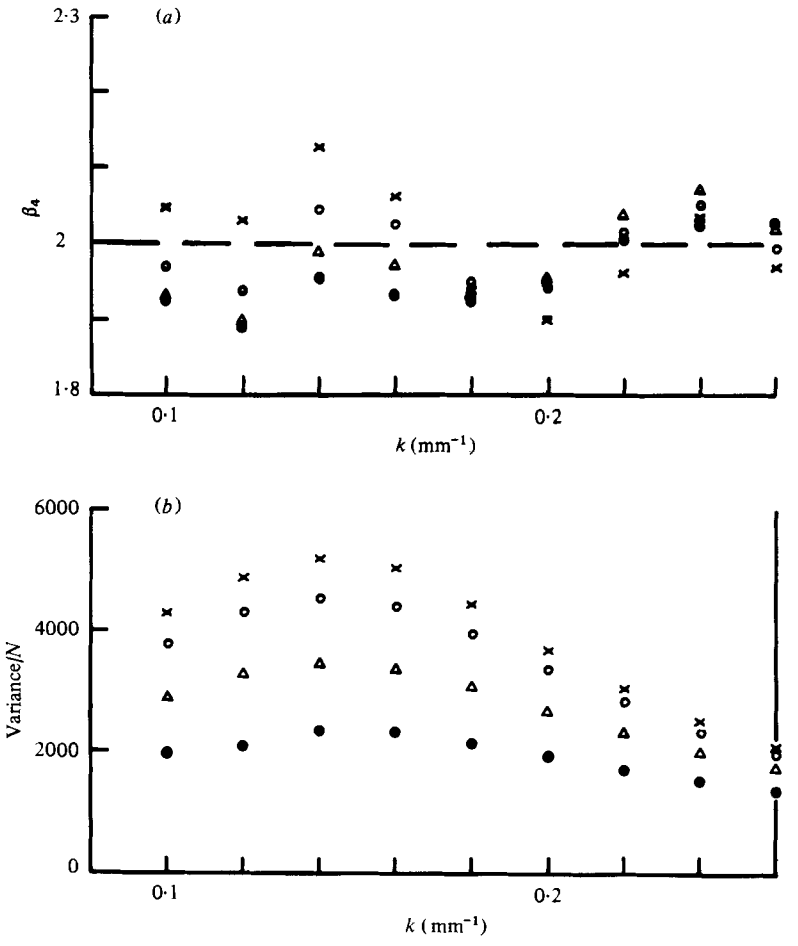

FIGURE 6. Evidence for long roller eddies in the boundary layer from statistics of the amplitudes of the Fourier coefficients of time-averaged fluctuations: (*a*) kurtosis, (*b*) variance, as functions of the transverse wavenumber. ●, $N=4$; △, $N=8$; ○, $N=16$; ×, $N=32$.

variation of the variance with sample number indicates effective lengths of order 200 mm.

The central wavenumber for the first group agrees well with the position of the first minimum of the transverse correlation function $R_{11}(0, r, 0)$ (figure 1), and the high value of the kurtosis may mean that the main turbulent eddies are discrete, non-overlapping structures with considerable variation in lateral scale.

The second group of longer eddies, whose lateral scale is somewhat greater than the layer thickness, may be the long eddies generated by the postulated flow instability, but the sensor positions are too few and too closely spaced to decide whether they occur as quasi-periodic groups or merely in pairs.

Visual confirmation of the interpretation may be found in figure 7, which shows a sequence of simultaneous velocity profiles in the $0y$ direction. The vertical separation of the profiles is such that the diagram may be regarded as a plot of the velocity fluctuations in the $x0y$ plane. An example of a long eddy pattern with a lateral wavelength of around six sensor separations is to be found in the left-hand column of

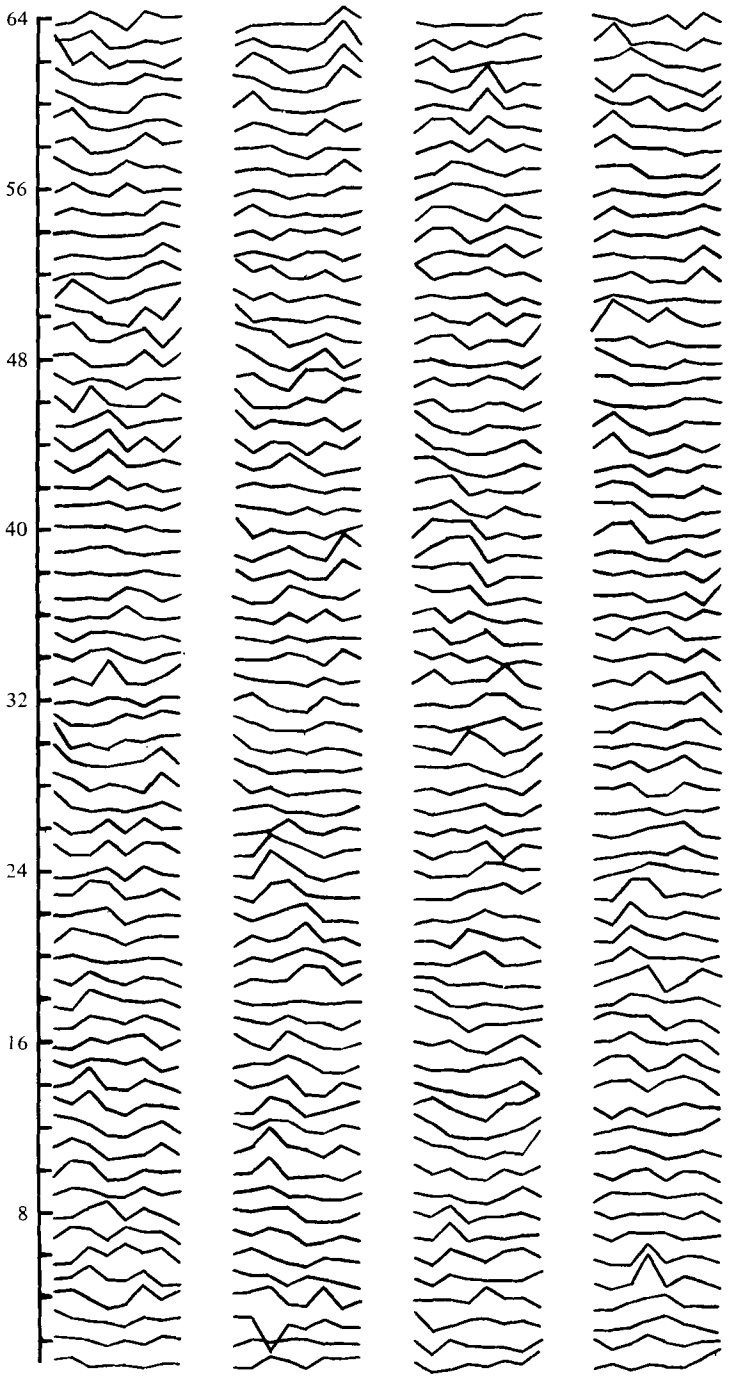

FIGURE 7. Instantaneous transverse profiles of streamwise fluctuations in the boundary layer at $z = 22{\cdot}6$ mm. The time interval between successive profiles is 1·024 ms, equivalent to 11 mm displacement in the direction of flow.

profiles, extending from profile number 9 to profile number 26 with minor lateral displacements of the maxima and minima and occasional obscuring by small-scale motions. An example of an eddy of the main motion, i.e. the first group, occurs in the second column from the left from profile number 36 to profile number 41.

5. The fitting of simple and weighted correlations by superposition of simple velocity patterns

If velocity patterns in the flow change very little as they sweep past the array of sensors, successive groups of sampled outputs are nearly simultaneous values of the fluctuations at positions displaced in the stream direction by the product of **U**, the mean velocity, and τ_s, the time interval between samples. That is to say, the fluctuation velocities recorded by the sensor at position $\mathbf{x}$ at times $t+n\tau_s$ are very nearly the fluctuations at time t for the series of positions $\mathbf{x}-\mathbf{U}n\tau_s$.

The availability of effectively simultaneous values for velocity fluctuations at many positions in the flow means that the velocity products used in the calculation of the correlation function $R(\mathbf{r},\mathbf{x})$ can be weighted in favour of special flow conditions within a considerable volume of the flow. The ordinary correlation function is calculated from the record as

$$R(\mathbf{r},\mathbf{x}) = \frac{1}{N}\sum_{n=1}^{N} v_n(\mathbf{x})\, v_n(\mathbf{x}+\mathbf{r}), \tag{5.1}$$

where $v_n(\mathbf{x})$ is the velocity fluctuation at (effective) position $\mathbf{x}$ for the nth sampling, while a weighted correlation is

$$Q(\mathbf{r},\mathbf{x}) = \sum_{n=1}^{N} v_n(\mathbf{x})\, v_n(\mathbf{x}+\mathbf{r})\, W_n \Big/ \sum_{n=1}^{N} W_n, \tag{5.2}$$

where W_n may depend on the fluctuations at all the data points used for velocity products in the nth sample.

If all the sensors are responding to the same component of the velocity fluctuation, an obvious weighting factor is

$$W_n = \sum_{\text{all } \mathbf{x}} v_n^2(\mathbf{x}), \tag{5.3}$$

the sum of the squares of the fluctuations at all the data points in the sampled volume, and it favours the eddy structures that contribute most to total intensity of the component within the volume. If the sensors respond to different components of the velocity fluctuation, more elaborate weighting schemes are possible. A useful configuration is a three-row array with sensor wires at 45° to the mean flow and orientated to be sensitive alternately to $(u+w)$ and to $(u'-w')$. If two neighbouring sensors are responding to $(u+w)$ and to $(u'-w')$, the difference of their squares is

$$(u+w)^2-(u'-w')^2 \simeq 2uw+2u'w' \tag{5.4}$$

and the sum of the differences for all pairs of points within the sampled volume is determined mostly by the contribution to the Reynolds shear stress from it.

In addition, by forming the quantities,

$$(u+w)^2+(u'-w')^2 \quad \text{and} \quad (u+w)(u'-w'),$$

and summing over the volume, weighting factors are found that favour sampled volumes that contribute most to the turbulent intensities, $\overline{u^2}$ and $\overline{w^2}$.

Most of the following results have been obtained from sample volumes containing 64 data points from eight equally spaced sample groups. Both the ordinary and weighted correlations have been calculated for the 2080 values of the sensor separation, and the results have been compared with correlation functions, $F(\mathbf{r};\mathbf{x})$, that would be found if the turbulence were entirely a superposition of eddies of simple form. A measure of the resemblance between a correlation function calculated from the data and one for an assembly of model eddies is provided by the matching coefficient,

$$J = \frac{\Sigma F(\mathbf{r};\mathbf{x})\, Q(\mathbf{r};\mathbf{x})\, B(\mathbf{r};\mathbf{x})}{[\Sigma F^2 B \times \Sigma Q^2 B]^{\frac{1}{2}}}, \tag{5.5}$$

where the sum is over all the sensor separations, and B is an additional weighting factor that may be used to favour velocity products for particular separations.

The procedure is to vary each parameter of the model eddy in rotation to produce a maximum value of the matching coefficient, continuing until no further increase can be obtained. If the entire turbulent motion were the superposition of randomly distributed model eddies, the final value of the coefficient would be one and the parameters would be those of the flow eddies. The degree of mismatch is to be measured by the difference of the coefficient from one.

Some likely causes of a mismatch are:

(i) The contribution to the correlation function from small, quasi-isotropic eddies of the dissipation chain.

(ii) Use of a model flow pattern that has very little in common with the turbulent flow.

(iii) A two-component structure of the main turbulent motion, e.g. entrainment eddies and double rollers in a wake.

(iv) Occurrence of a cycle of eddy growth and decay with substantially different flow patterns at different stages in the cycle.

Of these, the contribution from smaller eddies can be reduced by setting the weighting factor B less for small separations than for larger ones, the presence of two distinct kinds of eddy only complicates the problem by introducing more eddy parameters, while the flow patterns at a particular stage of a growth-decay cycle could be determined if a weighting factor could be devised specific to that stage. The weighting factors mentioned above may be regarded as aimed at discriminating between the stages with maximum Reynolds stress and maximum turbulent intensities.

6. Velocity patterns in the turbulent wake

The form of the velocity correlation function in many free turbulent flows suggests that the main motion may be composed of an assembly of inclined, double-roller eddies, with velocity distributions similar to that of the 'model' eddy,

$$\left.\begin{aligned} u &= (1-\beta^2y^2)\exp -\tfrac{1}{2}(\alpha^2x^2+\beta^2y^2+\gamma^2z^2+2\delta xz),\\ v &= y((\alpha^2+a\delta)\,x+(a\gamma^2+\delta)\,z)\exp -\tfrac{1}{2}(\alpha^2x^2+\beta^2y^2+\gamma^2z^2+2\delta xz),\\ w &= au. \end{aligned}\right\} \tag{6.1}$$

The model eddy may be described as a pair of oppositely rotating roller eddies with axes inclined to the flow direction at an angle of $\theta = \frac{1}{2}\arctan\,(2\delta/(\alpha^2-\gamma^2))$

and occupying a region similar in shape to but rather larger than the reference ellipsoid,

$$\alpha^2x^2+\beta^2y^2+\gamma^2z^2+2\delta xz = 1. \tag{6.2}$$

It is generally similar to the eddy sketched by Townsend (1976, p. 120†).

The nature of the eddy is more easily appreciated if it is specified by parameters of the reference ellipsoid, α_s, β_s, γ_s and θ, related to α, β, γ and δ by

$$\left.\begin{aligned}\alpha^2 &= \alpha_s^2\cos^2\theta+\gamma_s^2\sin^2\theta,\\ \beta &= \beta_s,\\ \gamma^2 &= \alpha_s^2\sin^2\theta+\gamma_s^2\cos^2\theta,\\ \delta &= (\alpha_s^2-\gamma_s^2)\sin\theta\cos\theta,\end{aligned}\right\} \tag{6.3}$$

and defining the magnitudes and orientation of the principal axes.

If the motion were the result of superimposing velocity distributions of the form (6.1) with centres distributed randomly over a plane $z = z_0$, the correlation function, $R_{ij}(\mathbf{r};\mathbf{x}) = \overline{u_i(\mathbf{x}+\frac{1}{2}\mathbf{r})\,u_j(\mathbf{x}-\frac{1}{2}\mathbf{r})}$, would have components,

$$\left.\begin{aligned}R_{11}(\mathbf{r};z) &= \tfrac{3}{4}(1-\beta^2r_2^2+\tfrac{1}{12}\beta^4r_2^4)\times E,\\ R_{22}(\mathbf{r};z) &= \tfrac{1}{2}\beta^{-2}(1-\tfrac{1}{2}\beta^2r_2^2)\,[C^2(z^2-\tfrac{1}{4}r_3^2)\\ &\quad -\tfrac{1}{2}\alpha^{-2}A^2(1-\tfrac{1}{2}\alpha^2(r_1+Br_3)^2)-\tfrac{1}{2}CAr_3(r_1+Br_3)]\times E,\\ R_{12}(\mathbf{r};z) &= r_2(\tfrac{3}{4}-\tfrac{1}{8}\beta^2r_2^2)\,[C(z-\tfrac{1}{2}r_3)-A(r_1+Br_3)]\times E\\ &= R_{21}(-\mathbf{r};z),\\ R_{13}(\mathbf{r};z) &= R_{31}(\mathbf{r};z) = aR_{11}(\mathbf{r};z),\\ R_{33}(\mathbf{r};z) &= a^2R_{11}(\mathbf{r};z),\end{aligned}\right\} \tag{6.4}$$

where

$$E = \exp-\tfrac{1}{4}(\alpha^2r_1^2+\beta^2r_2^2+\gamma^2r_3^2+2\delta r_1r_3)\exp-[(\gamma^2-\delta^2/\alpha^2)\,(z-z_0)^2],$$

$$A = \alpha^2+a\delta,\quad B = \delta/\alpha^2,\quad C = a(\gamma^2-\delta^2/\alpha^2).$$

Using the correlations from a particular record, the values of the eddy parameters were varied in rotation to give the best fit to the covariances of equations (5.4), the degree of fit being measured by the coefficient J of equation (5.5). In general, six parameters are available for the fitting but most sensor arrays provide no information about some of them, e.g. a linear array parallel to the $0z$ axis will not give useful values of β, and one with sensors responding to linear combinations of the u and w components cannot fix the value of a.

Some of the results are shown in table 1, which lists the optimum values of the relevant parameters and the coefficient of fit, J as defined by equation (5.5). A constant feature is that correlations weighted for total intensity over the sampled volume give consistently better coefficients of fit than the unweighted correlations with significantly different parameters. To the extent that the model velocity pattern of (6.1) is able to represent the actual patterns, it appears that eddies making large contributions to the intensity of a particular component of the fluctuations are more uniform in structure than the ensemble of eddies making some contribution. The implication is that each of the dominant, energy-containing eddies goes through a cycle of growth and decay with substantial changes in shape and velocity pattern during the life-time of each eddy.

(*a*) u-sensors linear arrays

File	Array	Weight	α	α_s	β	γ_s	θ	z_0	J
2	$0z$	N	28	23	—	47	0·40	20	0·930
		W	23	20	—	43	0·30	20	0·956
6	$0y$	N	26	26	21	26	(0·45)	20	0·952
	(z = 0)	W	24	26	20	9	(0·45)	20	0·966
9	$0y$	N	33	27	27	55	(0·40)	30	0·936
	(z = 20 mm)	W	30	23	26	55	(0·40)	25	0·950
12	$0y$	N	36	38	28	30	(0·50)	20	0·910
	(z = 40 mm)	W	32	32	26	30	(0·50)	20	0·924
48	$0z$	N	28	28	—	46	−0·05	14	0·928
	(Central)	W	24	24	—	44	0·05	10	0·957
52	$0y$	N	36	38	33	25	(0·50)	—	0·921
	(z = 0)	W	32	32	24	30	(0·50)	—	0·943
Mean values		N	31	33	25	41	0·30	17	
		W	27	28	24	39	0·30	15	

(*b*) $(u+w)$-sensors linear arrays

File	Array	Weight	α	α_s	β	γ_s	θ	z_0	J
39	$0y$	N	39	40	23	37	(0·70)	—	0·915
	(z = 0)	W	34	40	22	24	(0·70)	—	0·929
41	$0y$	N	35	42	28	55	(0·40)	—	0·910
	(z = 20 mm)	W	33	36	27	55	(0·40)	—	0·921

(*c*) $(u+v)$-sensors linear arrays

File	Array	Weight	α	α_s	β	γ_s	θ	a	z_0	J
24	$0y$	N	46	63	22	40	1·10	1·15	20	0·918
	(z = 0)	W	45	62	21	40	1·10	1·15	20	0·923
27	$0y$	N	43	30	36	62	0·60	0·80	25	0·922
	(z = 20 mm)	W	38	27	34	55	0·60	0·80	25	0·932

(*d*) 2:4:2 arrays

File	Sensors	Weight	α	α_s	β	γ_s	θ	a	z_0	J
1·11	u	N	38	37	33	57	0·20	(0·80)	20	0·922
		W	32	32	54	20	0·20	(0·80)	20	0·934
1·13	$(u+w)$	N	54	57	32	42	0·50	(0·80)	20	0·905
		W	46	50	31	37	0·65	(0·80)	25	0·920
1·16	$(u+w)$	N	53	57	32	42	0·55	(0·80)	20	0·924
		W	44	49	33	35	0·65	(0·80)	20	0·937
1·19	$(u+w)$	N	52	52	35	42	0·20	(0·80)	25	0·934
		W	45	45	33	39	0·25	(0·80)	25	0·948

(i) Entries omitted or in parentheses indicate that the sensor array does not discriminate between values of the parameter.

(ii) Effectively, $0y$ linear arrays can give information only concerning the parameters α and β, not α_s, γ_s and θ individually.

(iii) Units of α, α_s, β and γ_s are m^{-1}.

TABLE 1. Eddy parameters for the wake.

Sensors	Weight	α	α_s	β	γ_s	θ	α	z_0/l_0
u	N	0·84	0·89	0·67	1·11	0·40	—	0·63
	W	0·73	0·76	0·65	1·05	0·30	—	0·56
$(u+w)$	N	1·00	1·08	0·69	1·24	(0·40)	—	—
	W	0·90	1·03	0·66	1·07	(0·40)	—	—
$(u+v)$	N	1·20	—	0·78	—	—	0·98	—
	W	1·22	—	0·74	—	—	0·98	—
$(u+w)$	N	1·43	1·49	0·89	1·13	0·42	—	0·93
2:4:2 array	W	1·21	1·30	0·87	1·00	0·52	—	0·93

The reference length is $l_0 = 27$ mm, the 'standard deviation' of the mean velocity distribution.

TABLE 2. Non-dimensional parameters for the wake.

By using the scale width of the mean velocity distribution, l_0, defined to give the best fit between the distribution of mean velocity defect with

$$U_1 - U = u_0 \exp -\tfrac{1}{2}z^2/l_0^2 \tag{6.5}$$

the parameters may be expressed in non-dimensional form. The values given in table 2 are averages for broadly similar arrays of sensors.

Some direct evidence for the occurrence of eddy patterns of the double-roller type may be found in figure 8 which shows a series of instantaneous profiles of velocity fluctuation, obtained from a line of eight sensors in the $0y$ direction, responding to the $0x$ component of the velocity. Successive profiles are plotted at vertical intervals that represent the mean flow displacement over a sample interval on the same scale as the positions of the sensors. Patterns similar to those expected from the model eddies of equation (6.1) are frequent, persisting for about six samples – equivalent to a distance of about 70 mm – and broadly consistent with the eddy parameters found by the process of matching correlations (compare figure 9).

7. Velocity patterns in a boundary layer

For boundary layers, the model eddy of equation (6.1) does not satisfy the wall condition that the normal component of velocity should be zero there, and it should be replaced by one with a velocity distribution such as

$$\left.\begin{aligned} u &= z(1-\beta^2y^2)\exp -\tfrac{1}{2}(\alpha x^2+\beta y^2+\gamma^2z^2+2\delta xz),\\ v &= y(1-(\alpha^2+a\delta)\,xz-(a\gamma^2+\delta)\,z^2)\exp -\tfrac{1}{2}(\alpha^2x^2+\beta^2y^2+\gamma^2z^2+2\delta xz),\\ w &= au. \end{aligned}\right\} \tag{7.1}$$

This 'attached' eddy extends from the wall to a distance of order $(\gamma^2-\delta^2/\alpha^2)^{-\frac{1}{2}}$, and it has a roughly ellipsoidal shape with principal axes in the $0y$ direction and at angles θ and $(\theta+\frac{1}{2}\pi)$ to the flow direction, where

$$\tan 2\theta = 2\delta/(\alpha^2-\gamma^2). \tag{7.2}$$

In boundary layers and other wall flows, attached eddies of different sizes are to be found and the effects of the variation in size become important near the wall. Further, turbulence composed of eddies of a single simple kind would have a distribution of Reynolds stress of the form $z^2\exp(-Cz^2)$, very different from the real distribution

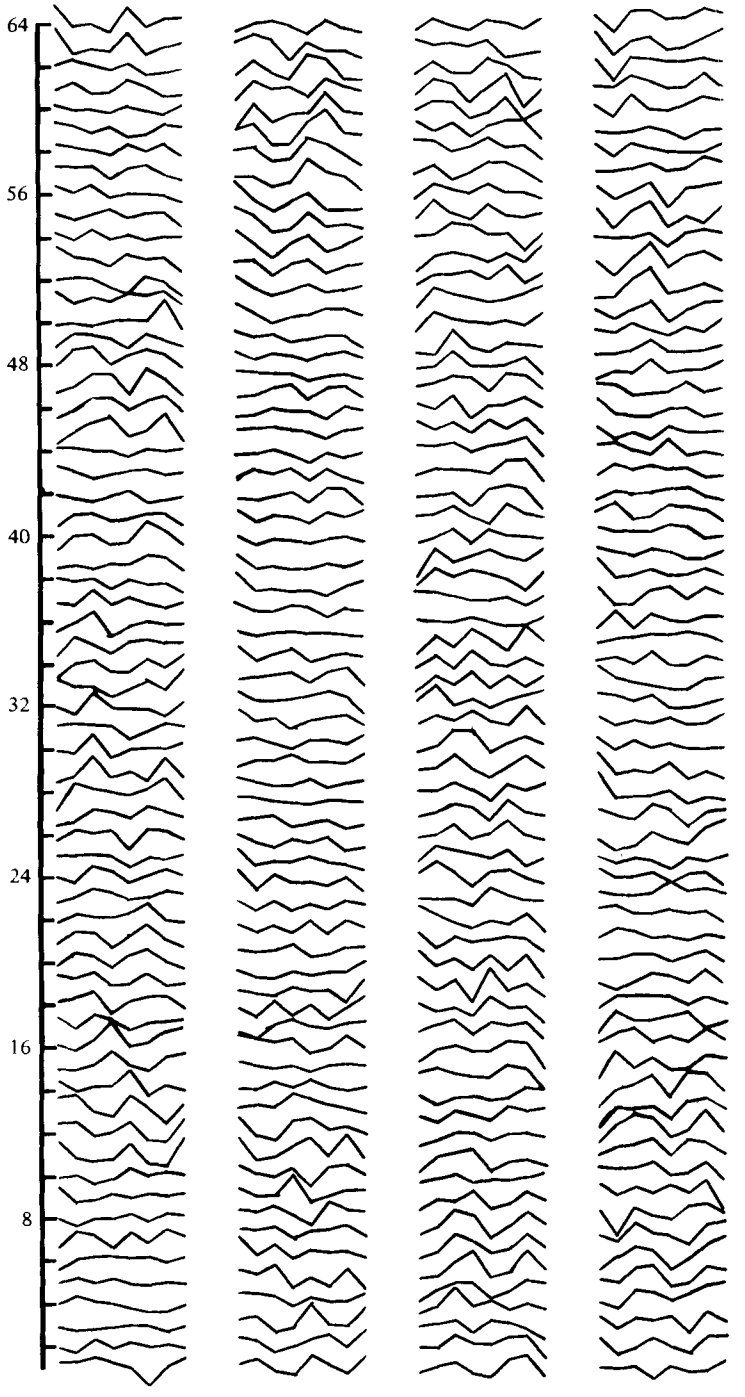

FIGURE 8. Instantaneous transverse profiles of streamwise fluctuations in the wake for $z = 20$ mm. The time interval between successive profiles is 1·024 ms, equivalent to 11 mm displacement in the direction of flow.

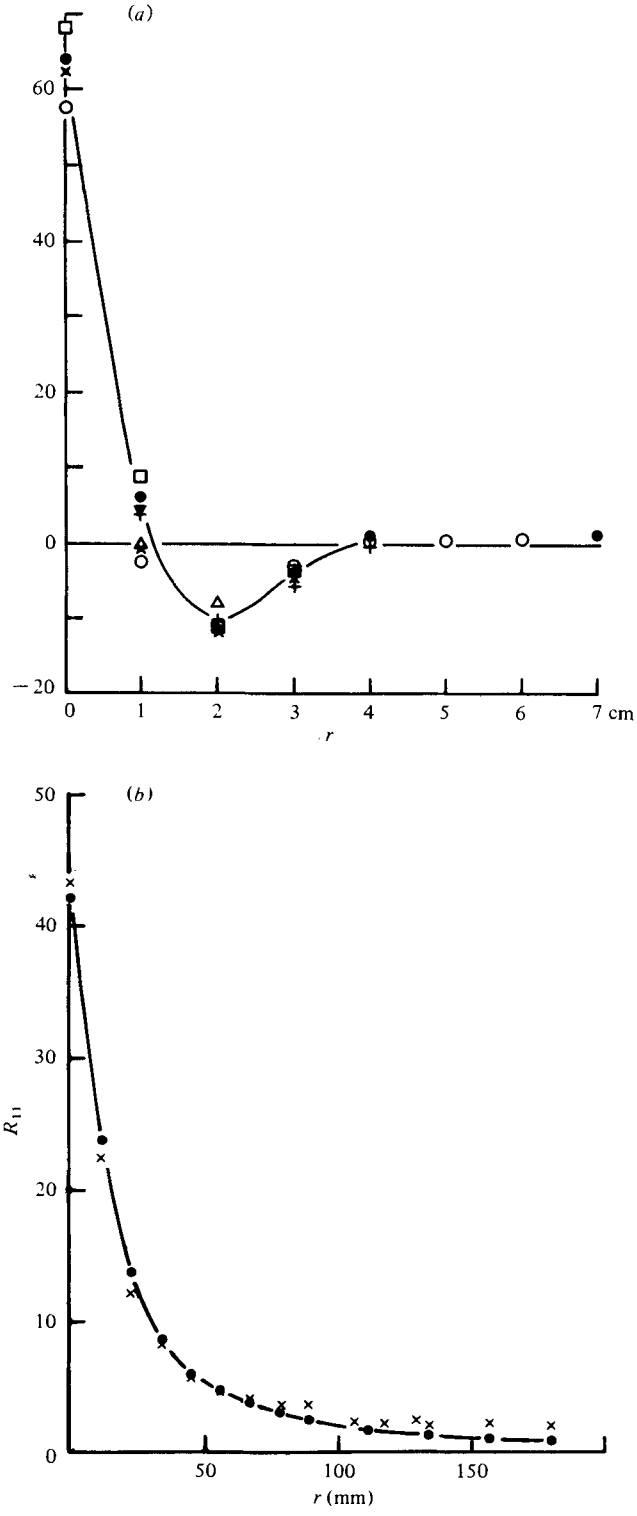

FIGURE 9. Correlation functions measured in the boundary layer. (*a*) Transverse component $R_{11}(0, r, 0; z)$ for $z = 17$ mm; (*b*) longitudinal component $R_{11}(r, 0, 0; z)$ for $z = 22{\cdot}6$ mm (●) and $z = 35{\cdot}3$ mm (×). (Note the change of vertical scale in (*b*). Units of R_{11} are $10^{-4}U_1^2$.)

which is roughly of the form $\exp(-Cz^2)$. It is more realistic to postulate that the whole motion of the layer resembles that of an ensemble of eddies of the form (7.1), with centres randomly distributed in the $x0y$ plane and with size parameters of all values from small ones that refer to the largest eddies to small ones that refer to attached eddies comparable in size with the thickness of the viscous layer. For simplicity, the ratios of the parameters, α, β, γ and δ, are kept the same for all the model eddies, and the size distribution is chosen so that the calculated distribution of Reynolds stress for the model flow becomes

$$R_{13}(0; z) = \text{constant} \times \exp -(\gamma^2 - \delta^2/\alpha^2) z^2, \tag{7.3}$$

where α, γ, δ are values for the largest of the attached eddies.

In the model flow, motion in the outer layer is determined almost entirely by the largest of the component eddies (7.1), while the motion in the inner layer depends on eddies of all sizes from those comparable with distance from the wall to the largest eddies of the flow. Within the inner layer, large eddies of scale comparable with the flow width contribute only to the u and v fluctuations and play no role in the transport of momentum or turbulent energy dissipation, i.e. they have no influence on the local similarity. In terms of the two-layer description, the outer layer is distinguished by a limited range of eddy size in contrast to the inner layer containing eddies with a wide range of sizes (Townsend 1976, chap. 5).

Using the size distribution that leads to the error-law distribution of Reynolds stress, the components of the correlation function may be calculated. They are

$$\left.\begin{aligned}
R_{11}(\mathbf{r}; z) &= \beta^2(z^2 - \tfrac{1}{4}r_3^2)\,[\tfrac{3}{4} - \tfrac{3}{4}\beta^2 r_2^2(1 + Q_0^{-1}) \\
&\qquad + \beta^4 r_2^4(1 + 2Q_0^{-1} + 2Q_0^{-2})]\, e^{-Q_0}/Q_0, \\
R_{22}(\mathbf{r}; z) &= \tfrac{1}{2}Ei(Q_0) + [(L - \tfrac{1}{4}\beta^2 r_2^2) + (M - \tfrac{1}{4}\beta^2 r_2^2 L) \\
&\qquad \times (1 + Q_0^{-1}) - \tfrac{1}{4}\beta^2 r_2^2 M(1 + 2Q_0^{-1} + 2Q_0^{-2})]\, e^{-Q_0}/Q_0, \\
R_{12}(\mathbf{r}; z) &= -\beta_0^2 r_2(z + \tfrac{1}{2}r_3)\,(\tfrac{3}{4} - (\tfrac{1}{8}\beta^2 r_2^2 + \tfrac{3}{4}N)\,(1 + Q_0) \\
&\qquad + \tfrac{1}{8}\beta^2 r_2^2 N(1 + 2Q_0^{-1} + 2Q_0^{-2}))\, e^{-Q_0}/Q_0, \\
R_{13}(\mathbf{r}; z) &= R_{31}(\mathbf{r}; z) = aR_{11}(\mathbf{r}; z), \\
R_{33}(\mathbf{r}; z) &= a^2 R_{11}(\mathbf{r}; z),
\end{aligned}\right\} \tag{7.4}$$

where
$$\begin{aligned}
Q_0 &= \tfrac{1}{4}(\alpha^2 r_1^2 + \beta^2 r_2^2 + \gamma^2 r_3^2 + 2\delta r_1 r_3) + (\gamma^2 - \delta^2/\alpha^2) z^2, \\
L &= -C(z^2 + \tfrac{1}{4}r_3^2) + \tfrac{1}{4}\alpha^{-2}A^2(z^2 - \tfrac{1}{4}r_3^2) + \tfrac{1}{4}Ar_3(r_1 + Br_3), \\
M &= C^2(z^2 - \tfrac{1}{4}r_3^2)^2 - \tfrac{1}{4}A^2(r_1 + Br_3)^2\,(z^2 - \tfrac{1}{4}r_3^2) + \tfrac{1}{4}ACr_3(r_1 + Br_3)\,(z^2 - \tfrac{1}{4}r_3^2), \\
A &= \alpha^2 + a\delta, \quad B = \delta/\alpha^2, \quad C = a(\gamma^2 - \delta^2/\alpha^2), \\
N &= C(z - \tfrac{1}{2}r_3)^2 + \tfrac{1}{2}A(r_1 + Br_3)\,(z - \tfrac{1}{2}r_3).
\end{aligned}$$

The calculated correlations have a single scale factor. The intensities and Reynolds stresses should be multiples of the correlation components for $\mathbf{r} = 0$, i.e.

$$\left.\begin{aligned}
R_{11}(0; z) &= \frac{3}{4}\frac{\beta_0^2}{\gamma^2 - \delta^2/\alpha^2}\exp -[(\gamma^2 - \delta^2/\alpha^2) z^2], \\
R_{22}(0; z) &= \tfrac{1}{2}Ei((\gamma^2 - \delta^2/\alpha^2)^{\frac{1}{2}} z) + (\tfrac{1}{4}\alpha^{-2}A^2 - C)/(\gamma^2 - \delta^2/\alpha^2)\exp -[(\gamma^2 - \delta^2/\alpha^2) z^2], \\
R_{33}(0; z) &= a^2 R_{11}(0; z), \\
R_{13}(0; z) &= aR_{11}(0; z).
\end{aligned}\right\} \tag{7.5}$$

(*a*) u sensors

File	Array	Weight	α_s	β_s	γ_s	θ	a	J
3	$0y$	N	68	78	74	0·2	—	0·842
	(z = 29·0 mm)	W	64	76	72	0·2	—	0·845
5	$0y$	N	58	70	34	0	—	0·898
	(z = 22·6 mm)	W	48	62	28	0·2	—	0·907
7	$0y$	N	52	68	42	0·2	—	0·926
	(z = 16·2 mm)	W	46	64	38	0·2	—	0·929

(*b*) $(u+w)$ sensors

File	Array	Weight	α_s	β	γ_s	θ	a	J
13	$0y$	N	106	82	30	0·28	—	0·821
	(z = 29·0 mm)	W	88	62	18	0·50	—	0·850
15	$0y$	N	98	92	46	0·02	—	0·875
	(z = 22·6 mm)	W	78	76	32	0·04	—	0·894
19	$0y$	N	56	82	74	0·30	—	0·928
	(z = 9·9 mm)	W	50	74	60	0·26	—	0·931
41	2:4:2	N	30	86	116	0·28	—	0·862
		W	32	84	134	0·32	—	0·874

(*c*) $(u+v)$ sensors

File	Array	Weight	α_s	β	γ_s	θ	a	J
25	$0y$	N	56	66	26	—	—	0·840
	(z = 22·6 mm)	W	44	52	18	—	—	0·855
29	2:4:2	N	22	58	180	0·45	−0·40	0·890
		W	24	58	156	0·40	−0·40	0·878
53	2:4:2	N	20	54	172	0·40	−0·55	0·877
		W	20	54	160	0·40	−0·55	0·858

(*d*) $(u+w)$ sensors

File	Array	Weight	α_s	β	γ_s	θ	a	J
44	2:4:2	N	88	96	84	0·65	0·20	0·890
		W(uw)	42	80	78	0·20	−0·65	0·943
		W(w^2)	66	96	80	0·20	−0·20	0·912
		W(u^2)	48	78	86	0·25	−0·20	0·912
46	2:4:2	N	52	90	97	0·35	−0·20	0·855
		W(uw)	41	94	103	0·35	−0·65	0·924
		W(w^2)	44	96	106	0·35	−0·20	0·862
		W(u^2)	44	81	115	0·35	−0·15	0·869

TABLE 3. Eddy parameters for the boundary layer.

In table 3, optimum values of the eddy parameters and the corresponding coefficients of fit are listed for various weightings and sensor cofigurations. Unlike the results for the wake, the coefficients of fit are much the same for all the records from the linear arrays, whether the correlations are weighted or unweighted, and the more interesting results are from three-row, 2:4:2 arrays with the sensors responding alternately to $(u+w)$ and to $(u-w)$. For these records, the eddy parameters for correlations weighted for uw are considerably different from those for correlations either unweighted or weighted for u^2 or w^2, and the coefficients of fit (J) are larger. The largest differences are in the parameter a, defining the plane of circulation in the model eddy.

The results are consistent with the view that the eddies go through a cycle of growth, decay and renewal that correspond with the bursts and sweeps described in the literature. Since the eddy forms are different at the various stages of the cycle, the larger coefficient of fit for weighting with Reynolds stress implies more uniformity of the eddies contributing to the stress, i.e. stress-producing flow is present for a comparatively short time during each cycle. This is consistent with the 'intermittency' of positive values of the velocity product, $-uw$, reported by several authors.

8. Discussion

The object of the experimental programme has been to identify coherent, organized eddy structures in turbulent shear flows by the analysis of recorded velocity fluctuations at points distributed over a substantial volume of the flow. There have been many studies made of organized eddies, particularly in boundary layers and jets using visualization and conditioned sampling techniques, and they have two characteristic features: (i) they are mutually exclusive to the extent that the flow fields of different eddies do not overlap appreciably, and (ii) they are not constant in form but go through a cycle of growth, decay and renewal. Since the flow fields do not overlap, the spatial distribution of the eddy centres cannot be random and, even if a sufficient knowledge of the correlation function were available, the eigenfunction method of Lumley (1965) is not strictly applicable. In addition, the variation of form over the growth–decay–renewal cycle means that any structure inferred from the correlation function is a blurred superposition of the various structures assumed by the eddy during the cycle.

The common feature of the methods used here to identify organized eddies may be described as conditional sampling with the condition referring to velocity fluctuations within a substantial volume of the flow rather than at or near a point. For the quasi-periodic entrainment eddies of the wake, the complexity of the velocity pattern leads to fairly accurate determination of its characteristics but it is less easy to obtain details of the main eddies of wakes and boundary layers. Although the correlations have been fitted with double-roller eddies, the present method is hardly able to distinguish between single and double rollers, and the significant parameters are the coefficients describing the spatial extent of the eddy and the plane of circulation. A next step is to match velocity patterns in the flow to a model eddy with parameters found by correlation matching and then, whenever the coefficient of fit is satisfactorily large to record both the actual pattern within the volume of fit and the pattern in the surrounding fluid. By using this form of conditional sampling. it is possible both to amend the model eddy to make it a better match to real velocity patterns and to discover the spatial relations and forms of neighbouring eddies. Work on these lines is now in progress.

On the whole, the results support the view that large-scale velocity patterns of the main turbulence are fairly simple but that time-averaging makes them appear more complex because of the superposition of patterns from eddies at all stages of the growth–decay–renewal cycle. Both for the wake and for the boundary layer, a good representation depends on using model eddies which extend across the whole flow (in the case of the wake, one-half of the flow). The good description of the wake by eddies of a single size with centres at a fixed distance from the central plane implies strong interactions between the whole of one side of the flow. For a realistic treatment of

unbounded shear flows, it seems preferable to avoid the use of 'local' equations for the turbulent Reynolds stresses with diffusion and 'scrambling' terms and to replace them with ones relating to the overall structure. Whether such an approach is practicable for purposes of prediction remains to be seen.

REFERENCES

BRADSHAW, P. 1965 *J. Fluid Mech.* **22**, 679.

BRADSHAW, P., FERRISS, D. H. & JOHNSON, R. F. 1964 *J. Fluid Mech.* **19**, 591.

BROWN, G. L. & ROSHKO, A. 1974 *J. Fluid Mech.* **64**, 775.

DAVIES, P. O. A. L. & YULE, A. J. 1975 *J. Fluid Mech.* **69**, 513.

FERNHOLTZ, H. 1964 *Aero. Res. Committee R. & M.* no. 3368.

GRANT, H. L. 1958 *J. Fluid Mech.* **4**, 149.

GUPTA, A. K., LAUFER, J. & KAPLAN, R. E. 1971 *J. Fluid Mech.* **50**, 493.

KEFFER, J. F. 1965 *J. Fluid Mech.* **22**, 135.

LUMLEY, J. L. 1965 Atmospheric Turbulence and Radio Wave Propagation. *Proc. Int. Colloq. Moscow*, p. 166.

TOWNSEND A. A. 1949 *Proc. Roy. Soc.* A **197**, 124.

TOWNSEND, A. A. 1970 *J. Fluid Mech.* **41**, 13.

TOWNSEND, A. A. 1976 *The Structure of Turbulent Shear Flow*. Cambridge University Press.